

# Design and Fabrication of a Composite Energy Absorber

**Hamidreza Shalian<sup>1</sup>, Mohsen Heydari Beni<sup>4</sup>**

Department of Mechanical Engineering,  
Malek Ashtar University of Technology, Tehran, Iran  
E-mail: [jejam@mail.com](mailto:jejam@mail.com), [Mohsenheydari1371@gmail.com](mailto:Mohsenheydari1371@gmail.com)

**Mohammad Hossein Alae<sup>2</sup>, Jafar Eskandari Jam<sup>3</sup>, \***

Department of Mechanical Engineering, Composite Engineering Research Institute  
Malek Ashtar University of Technology, Tehran, Iran  
E-mail: [mhallaee@mut.ac.ir](mailto:mhallaee@mut.ac.ir), [jafar.eskandarijam@gmail.com](mailto:jafar.eskandarijam@gmail.com)

\*Corresponding author

**Majid Eskandari Shahraki<sup>5</sup>, Naser Asiaban<sup>6</sup>**

Department of Aerospace Engineering,  
Ferdowsi University of Mashhad, Mashhad, Iran  
E-mail: [mjdeskandari@gmail.com](mailto:mjdeskandari@gmail.com), [naser.asiaban@mail.um.ac.ir](mailto:naser.asiaban@mail.um.ac.ir)

**Received: 5 April 2020, Revised: 4 August 2020, Accepted: 8 August 2020**

**Abstract:** In this paper, the quasi-static test and the damage of the thin-walled composite cylinder were numerically simulated using ABAQUS. Then, a comparison was made between the results of this simulation and those obtained from experimental studies followed by their validation. In the next step, several parameters affecting the energy absorption rate including outer diameter-to-cylinder height ratio, thickness-to-outer diameter ratio, and angle of damage initiation mechanism were selected. They were optimized by modelling different states in ABAQUS. The number of tests is reduced by the design of experiments using response surface methodology and the optimal specimen is extracted by this software. Finally, optimum adsorbent is fabricated and tested. Considering enhanced energy absorption, increased mean reaction force, and reduced initial maximum force, the optimal design parameters include the inner diameter-to-cylinder height ratio of 0.2, thickness-to-inner diameter ratio of 0.1, and angle of damage initiation mechanism of 45°.

**Keywords:** Composite, Crash Box, Energy Absorber, Quasi-Static

**Reference:** Hamidreza Shalian, Mohammad Hossein Alae, Jafar Eskandari Jam, Mohsen Heydari Beni, Majid Eskandari Shahraki, and Naser Asiaban, "Design and Fabrication of a Composite Energy Absorber", Int J of Advanced Design and Manufacturing Technology, Vol. 13/No. 4, 2020, pp. 1–12. DOI: 10.30495/admt.2020.1893677.1186

**Biographical notes:** **Hamidreza Shalian** received his MSc in Mechanical Engineering from University of Malek Ashtar. His field of research is mechanical analysis of composite materials. **Mohammad Hossein Alae** is currently Assistant Professor at the Department of Mechanical Engineering, at Malek ashtar University, Tehran, Iran. His current research interest includes composite manufacturing and composite structures. **Jafar Eskandari Jam** is Professor of Mechanical engineering at Malek Ashtar University, Tehran, Iran. His current research focuses on composite structures, plates and shell analysis and nanomechanics. **Mohsen Heydari Beni**, is currently a PhD student at Malek Ashtar University and his main research interests are composite structures, plates and shell analysis and nanomechanics. **Majid Eskandari Shahraki** is currently a PhD student at Ferdowsi University of Mashhad, Iran and his main research interests is nanomechanics. **Naser Asiaban** is currently a PhD student at Ferdowsi University of Mashhad, Iran. His field of research are simulation of Liquid Composite Molding (LCM) processes and renewable energies.

## 1 INTRODUCTION

Polymer composites are widely used in many industries such as aerospace, military, automotive, and so on due to their excellent mechanical properties, such as low strength-to-weight ratio. One of the inherent properties of these materials is high energy absorption. Energy absorption in polymer composite components depends on many parameters including fiber and matrix, fiber orientation angle, layer layout, and segment geometry. An ideal energy absorber should exhibit as much constant compressive force against the incoming force as possible. Under appropriate conditions, composite specimens exhibit this type of behavior as a progressive failure or stable crush. In contrast to progressive failure, there exists a catastrophic failure in which the response force has large amplitude oscillations. Figure 1 shows the force-displacement curves for an ideal, a metal and a composite material. The oscillations in the force-displacement curve of the metal are caused due to the folds in its structure [1].

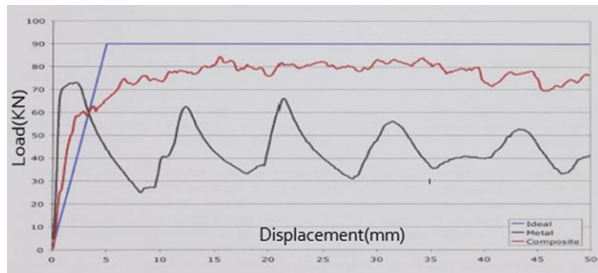


Fig. 1 Force-displacement curves for an ideal [1].

Figure 2a shows a specimen of the axially cut adsorbent tube. The specimen consists of a circular tube of length  $L$ , inner diameter  $D_1$ , and outer diameter  $D_2$ . A typical trigger mechanism generating a stable crush is shown at the top of the specimen at a 45-degree angle. The tube is assumed to lie between two flat planes at a certain displacement rate. If the composite tube experiences stable stiffness behavior, its post-crushing properties will be similar to “Fig. 2b”.

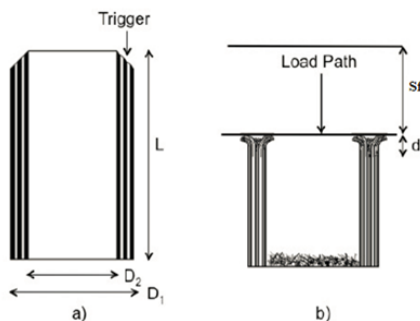


Fig. 2 Composite tube before and after stable crush [2].

In this case,  $S_f$  indicates the top plate displacement and  $d$  indicates the length of the crushing area. Figure 3 shows a typical force-to-displacement response for a composite tube having experienced stable crush. The curve with an initial linear loading area up to the maximum load caused by the local failure of the tube begins at the starting point of the tube. This point is marked on the graph with  $S_i$ . After the peak load, the stable crush region is determined by the tooth loads at an average constant load. Eventually, as the tube further crushes, the stiffness inside the tube begins to add up and the load increases. This displacement is indicated on the graph with  $S_b$  [2].

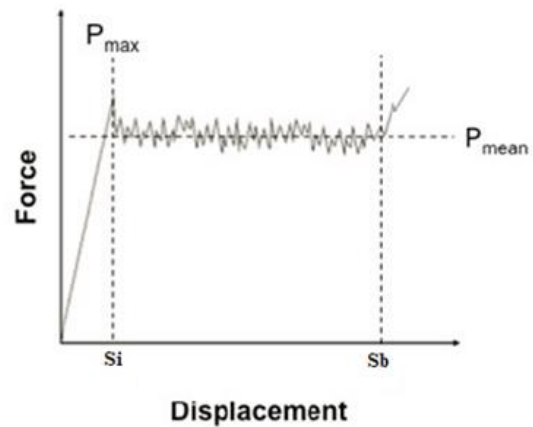


Fig. 3 Force-displacement curve for a composite tube [3].

The following force-displacement curve represents the total energy absorbed by the specimen, which can be expressed as Equation (1):

$$W = \int_0^{S_f} P ds \quad (1)$$

Where,  $W$  is the total energy absorbed during the crushing of the specimen,  $P$  is the crushing force, and  $S_f$  is the total displacement. Equation (2) can be used to better illustrate the properties of progressive crushing mode:

$$W = \int_0^{S_f} P ds = P_m (S_b - S_i) \quad (2)$$

Where,  $P_m$  is the average (mean) crushing load,  $S_i$  is the initial length of the crushed segment of the specimen, as shown in “Fig. 3”. Equation (3) is used to obtain specific energy absorption (SEA):

$$SEA = \frac{W}{m} \quad (3)$$

Where,  $m$  is the mass of the tube. By combining the two equations above, Equation (4) is obtained as follows:

$$SEA = \frac{W}{m} = \frac{P_m(S_b - S_i)}{V\rho} \quad (4)$$

Where,  $V$  is the volume and  $\rho$  is the density of the material. The above equation can be expressed as Equation (5):

$$SEA = \frac{W}{m} = \frac{P_m(S_b - S_i)}{V\rho} = \frac{P_m(S_b - S_i)}{AL\rho} \quad (5)$$

Where,  $A$  is the cross-sectional area and  $L$  is the length of the tube.  $S_i$  is very small, and is negligible when combined with  $S_b$ . The above equation can be rewritten as Equation (6):

$$SEA = \frac{P_m S_b}{AL\rho} \quad (6)$$

Hamada et al. [4] conducted a study on the use of a carbon-fiber-reinforced polyetheretherketone (PEEK) matrix, with an energy absorption exceeding 180 kJ/kg, more than twice that of carbon/epoxy. This is due to the improved properties of the PEEK matrix, with high resistance to crack growth between the fibers preventing failure, resulting in stable progressive crushing [5].

Ramakrishna [6] studied the performance of tubular composite adsorbents made of carbon fiber and various types of thermoplastic matrices including polyetheretherketone (PEEK), polyetherimide (PEI), polyimide (PI), and polyarylsulfone (PAS). The results show that PEEK has the highest SEA among the materials used, thanks to its high fracture toughness.

In a similar study, Sato et al. [7] studied thermoplastics composites (TMCs) including carbon-fiber-fabric reinforced polyetherimide (CF Fabric/PEI), carbon fiber reinforced polyimide (C/PI), carbon fiber reinforced polyarylsulfone (C/PAS), and carbon-fiber-reinforced polyetheretherketone (C/PEEK) as energy absorbers and compared them with carbon/epoxy and glass/epoxy. The results showed that carbon/thermoplastic tubes have higher energy absorption capability than carbon/thermoset tubes.

The fiber orientation angle greatly affects the energy absorption of composite tubes. Different laminates have been investigated for tubular adsorbent samples. The most common ones are  $[0/90]$   $[\theta \pm 0.0]$  usually created by roll wrapping or triaxial braided fabrics and  $[\pm\theta]$  made by filament winding or biaxial braided fabrics.

Farley [8] observed significant differences in the energy absorption process of these materials on glass/epoxy, carbon/epoxy, and Kevlar/epoxy with the  $[\theta \pm 0]_4$  fiber structure, with  $\theta$  varying between  $0/90^\circ$  degrees. The differences in the energy absorption process in this study can be justified by examining the crushing modes of the specimens. The results indicated an increase in the SEA of the glass/epoxy and Kevlar/epoxy tubes with an increase in the fiber orientation angle ( $\theta$ ).

Farley and Jones [9] tested several specimens of carbon/epoxy and glass/epoxy tubes designed with a fiber structure  $[\theta \pm 0]$  to investigate the effect of fiber orientation on energy absorption capability. The results showed a decrease in the energy absorption capability of the non-linear carbon/epoxy tube with a brittle fracture mode with an increase in  $\theta$ . Furthermore, the glass/epoxy cylinder energy absorption capability increases nonlinearly with an increase in  $\theta$ . In this research, the crushing mode of glass/epoxy tube of bending layers is observed.

Hamada et al. [10] studied the effects of fiber alignment on the energy absorption capability of carbon fiber and polyethylene-reinforced epoxy resin hybrid composite tubes. The results suggested an increase in energy absorption capability with an increase in the fiber orientation angle to the longitudinal axis of the tube.

Ramakrishna et al. [11] studied the energy absorption rate of carbon fiber-reinforced composite tubes with different thermoplastic matrices including polyetheretherketone (PEEK), polyetherimide (PEI), polyimide (PI), and polyarylsulfone (PAS). In their research, they used fiber alignment as  $0, \pm 5, \pm 10, \pm 15, \pm 20, \pm 25$ , and  $\pm 30$  degrees relative to the tube axis. Their results generally indicated a decrease in longitudinal cracks with an increase in  $\theta$ , due to increased fracture toughness with an increase in  $\theta$ . This improved fracture toughness results in greater crack growth resistance and consequently increased the SEA for the composite material. Microfracture processes such as fiber fracture increase with an increase in  $\theta$ . Therefore, it is concluded that these enhanced processes cause an increase in total energy absorption.

Several studies have explored the effects of using different fibers on the energy absorption rate of composite tubes. Unidirectional (UD) fiber fabrics have been shown to have a higher SEA potential than  $0/90^\circ$  fabrics. However,  $0/90^\circ$  fabrics are still used today in some cases due to cost considerations and simple production in low circulation [12-13]. Consequently, Kindervater [14] reported that tubes made of  $0/90^\circ$  carbon fabrics generally had lower SEAs than tubes made of prepreg unidirectional fabrics. He also managed to increase the SEA of circular and square tubes made of  $0/90^\circ$  fabrics by replacing several inner layers with  $0^\circ$  fibers.

Pafitis and Hall [15] showed that the force-displacement curve of cone-shaped composite tubes can be linear or exponential by changing the cone dimensions. Moreover, it was observed that these adsorbents showed higher energy absorption than constant intersecting values in non-axial tests [16]. Nevertheless, many researchers [17-19] have reported that the SEA decreases with an increase in the cone angle.

In this paper, the composite cylinder is numerically modeled under axial pressure in Abaqus and validated

by referring to experimental papers. Then, based on the studies, the materials and parameters affecting energy absorption are investigated. Finally, these parameters are optimized and the optimum adsorbent specimen is fabricated and tested.

## 2 SIMULATION AND NUMERICAL ANALYSIS

This section briefly addresses modeling based on experimental work by Hong et al. [20]. The results of the software simulation are validated with the results of this paper [20].

The specimens tested in Hang's study are T700/QY8911 composite cylindrical tubes with a uniform length of  $100 \pm 0.2$  mm and an inner diameter of 50 mm. The thickness of the tube consists of 14 layers of fabric with a thickness of 0.15 and the corresponding laminate is [0 90 0 0 90 - 45 +45]s. The trigger mechanism is a 45-degree chamfer, used as an important factor in producing gradual crushing and obtaining acceptable energy absorption from a circular tube at an axial load. "Table 1" shows the initial properties of the materials used in the composite tube in their research.

**Table 1** Initial properties of materials used for T700/QY8911 composite tube fabrication [20]

| Symbol   | Title   | Value | Unit            |
|----------|---|-------|-----------------|
| $\rho$   | Density   | 1.53  | $\text{g/cm}^3$ |
| $E_a$    | Young's modulus along the fiber direction                 | 135   | GPa             |
| $E_b$    | Young's modulus perpendicular to the fiber direction      | 9.12  | GPa             |
| $G_{ab}$ | Shear modulus on plane AB                                 | 5.67  | GPa             |
| $\nu$    | Poisson's ratio   | 0.021 | -               |
| $X_t$    | Tensile strength along the fiber direction                | 2326  | MPa             |
| $X_c$    | Compressive strength along the fiber direction            | 1236  | MPa             |
| $Y_t$    | Tensile strength perpendicular to the fiber direction     | 51    | MPa             |
| $Y_c$    | Compressive strength perpendicular to the fiber direction | 209   | MPa             |
| $S_c$    | Shear strength on plane AB                                | 87.9  | MPa             |
| $S_b$    | Interlayer shear strength                                 | 99.2  | MPa             |

In this study, quasi-static experiments were performed on a composite tube axially at room temperature under load at a rate of 2 mm/min [20]. Figure 4 shows the specimen image after damage.

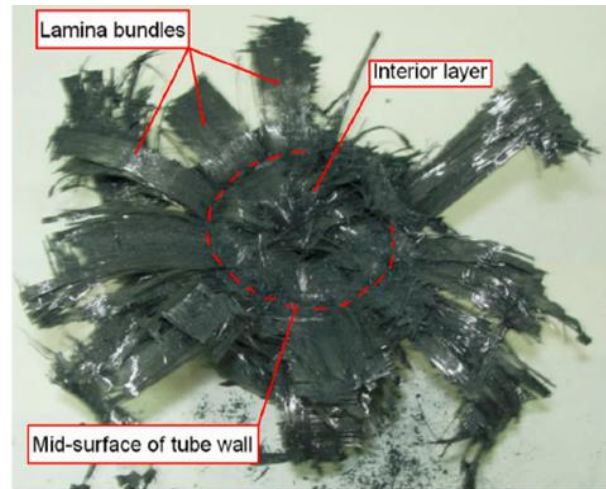


**Fig. 4** T700/QY8911 composite tube specimen after damage [20].

Figure 5 shows the specific stress-displacement curve of the T700/QY8911 composite tube specimen under quasi-static loading.

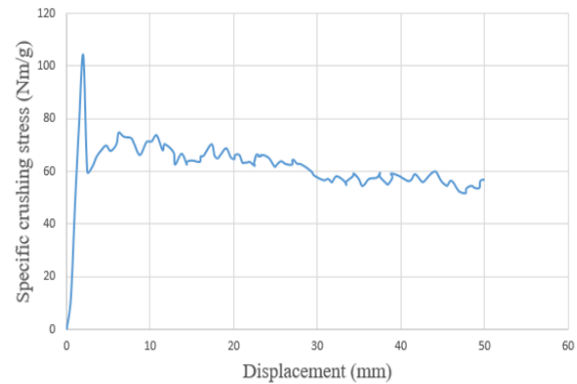


**Fig. 5** Specific stress-displacement curve of T700/QY8911 composite tube [20].

First, the composite energy absorber is simulated based on the specimen dimensions in [20], comprising three main components, namely the composite cylinder, the rigid loading plate, and the terminal static rigid plate. Specifications of the simulated composite cylinder model were 50 mm inner diameter, 100 mm height, and 0.15 mm layer thickness. Depending on the number of layers (i.e., 14), the total thickness of the cylinder is 2.1 mm. An appropriate damage initiation mechanism can reduce the maximum impact load, control the initial failure mode of the energy-absorbing components, and improve the energy absorption capability of the composite through gradual failure. Thus, a 45-degree chamfer is defined for the composite tube, as shown in "Fig. 6". To do so, three solid and deformable layers with different heights are used.

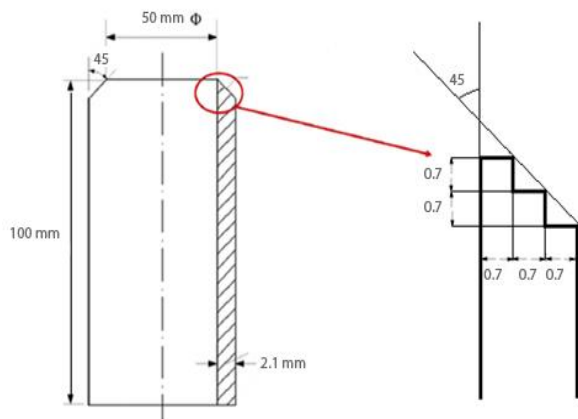


Fig. 6 Details of the simulated geometric model.

In this simulation, loading is performed by a rigid flat plate that applies the load on the model in a quasi-static manner.

A load is applied perpendicular to the force-exerting in the negative z-direction. This load is assumed to be of a constant velocity of 0.033 mm/s, equivalent to 2 mm/min (“Fig. 7”). Additionally, under boundary conditions, all degrees of freedom (DOFs) of the rigid loading plate are closed.

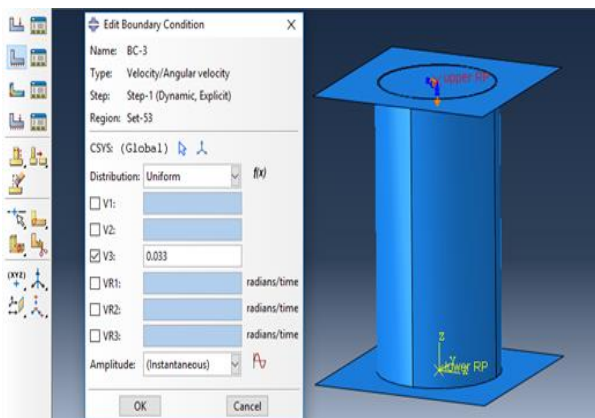


Fig. 7 Definition of the desired software loading.

The mesh size and number of elements have a direct impact on the accuracy of Abaqus results. Consequently, the element for which accurate results are obtained from the software must be applied to the segment. First, the meshing was applied with a coarse mesh (10600 elements). A few steps of mesh analysis and making the mesh finer resulted in the size (51762 elements) after which no change occurred in the amount of output support force (“Fig. 8”). SC8R square type elements were used for analysis.

The model was validated by being compared to the experimental results obtained by Hong et al. Then, the composite absorbent cylinder was optimized in order to improve energy absorption which means increasing the mean force, and decreasing the initial maximum force to

show a constant compressive force against the applied force [1].

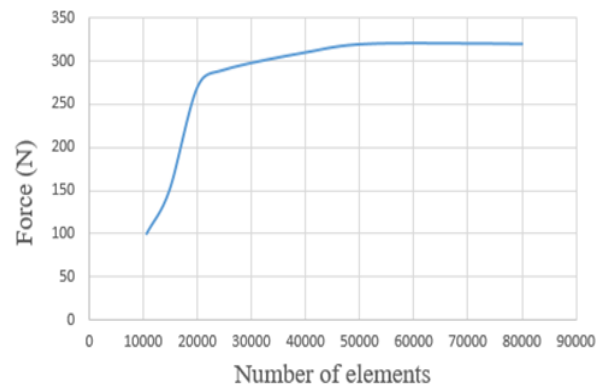


Fig. 8 Sensitivity of the mesh of the composite cylinder diagram.

To do so, the experimental design was used to save time and reduce the simulation time. Figure 9 shows the damage steps of this analysis.

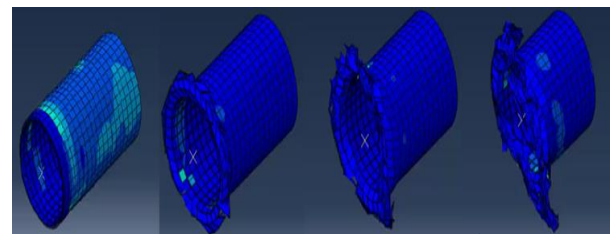


Fig. 9 Numerical model prototype at various stages of damage.

### 3 EXPERIMENTAL DESIGN AND SET-UP

In today's engineering world, the design of experiments is regarded as a vital tool for improving the performance of production processes. This study used carbon/epoxy composite, with its properties presented in “Table 2” according to the tests performed. Carbon is of 100g T300 fine-spun fabric type and epoxy is of room temperature vulcanized type manufactured in 2017. The height of all cylinders are 200 mm, a constant value. Three levels are considered for the diameter-to-tube length ratio, the thickness-to-inner diameter ratio of the tube, and the angle of damage initiation mechanism. The parameter levels are assumed to be 0.2, 0.15, and 0.1 for the inner diameter-to-height ratio of the tube and 0.1, 0.08, and 0.06 for the thickness-to-inner diameter ratio of the tube, respectively. In addition, angles of 20, 40, and 60 degrees are intended for the initiation mechanism of damage. Given the high number of full factorial experiments (i.e., 27), this study utilized the experimental design using response surface methodology to save time.

**Table 2** Initial properties used for modeling of carbon/epoxy composite tube

| Property | Description   | Value | Unit              |
|----------|---|-------|-------------------|
| $\rho$   | Density   | 1.64  | g/cm <sup>3</sup> |
| Ea       | Young's modulus along the fiber direction                 | 82    | GPa               |
| Eb       | Young's modulus perpendicular to the fiber direction      | 3.22  | GPa               |
| Gab      | Shear modulus on plane AB                                 | 4.5   | GPa               |
| $\nu$    | Poisson's ratio   | 0.2   | -                 |
| Xt       | Tensile strength along the fiber direction                | 680   | MPa               |
| Xc       | Compressive strength along the fiber direction            | 570   | MPa               |
| Yt       | Tensile strength perpendicular to the fiber direction     | 49    | MPa               |
| Yc       | Compressive strength perpendicular to the fiber direction | 43    | MPa               |
| Sc       | Shear strength on plane AB                                | 73.6  | MPa               |
| Sb       | Interlayer shear strength                                 | 96.7  | MPa               |

#### 4 RESPONSE SURFACE METHODOLOGY

Response Surface Methodology (RSM) is a set of mathematical methods that determine the relationship between one or more response variable(s) and several independent variables (case study). This method was introduced in 1951 by R. Wilson. It has been used to date as one of the tools of the design of experiments.

#### 5 PARAMETER SELECTION

This study investigated the effects of three input parameters, i.e., the height-to-inner diameter ratio of the tube, the inner diameter-to-thickness ratio of the tube, and the angle of damage initiation mechanism on three output parameters, i.e., specific energy absorption, initial peak load rate, and average load. Therefore, the design of experiments is used to reduce the number of simulation model runs. Under normal conditions, to perform a full factorial,  $3^3 = 27$  specimens need to be performed, reduced to 15 using the design of

experiments method. This process is done using the Design Expert software.

#### 6 THE STEPS OF DESIGN OF EXPERIMENTS

The design of experiments is performed using the RSM with a central composite design. The central mode is used when the distance between different levels of a parameter is equal.

#### 7 THE STEPS OF DESIGN OF EXPERIMENTS

Based on the performed experimental designs, 15 experiments were considered for this design, with five repeated experiments, as shown in "Fig. 10".

Finally, the 15 experiments proposed by the design of experiments were described and simulated similarly. Then, the results were fed into Design Expert software and one model was selected as the optimal specimen. The optimal specimen was constructed and evaluated in the next step to verify the DOE results.

| Run | Factor 1<br>A:D/L | Factor 2<br>B:t/D | Factor 3<br>C:Trigger an<br>degree |
|-----|-------------------|-------------------|------------------------------------|
| 1   | 0.2               | 0.08              | 40                                 |
| 2   | 0.15              | 0.08              | 40                                 |
| 3   | 0.15              | 0.08              | 40                                 |
| 4   | 0.1               | 0.06              | 20                                 |
| 5   | 0.15              | 0.08              | 60                                 |
| 6   | 0.15              | 0.08              | 40                                 |
| 7   | 0.15              | 0.08              | 20                                 |
| 8   | 0.1               | 0.08              | 40                                 |
| 9   | 0.1               | 0.1               | 60                                 |
| 10  | 0.15              | 0.08              | 40                                 |
| 11  | 0.15              | 0.06              | 40                                 |
| 12  | 0.2               | 0.1               | 20                                 |
| 13  | 0.15              | 0.1               | 40                                 |
| 14  | 0.15              | 0.08              | 40                                 |
| 15  | 0.2               | 0.06              | 60                                 |

**Fig. 10** Determination of the number of experiments required for the design of experiments performed.

#### 8 OPTIMAL SPECIMEN FABRICATION

Finally, the optimal specimen was constructed according to the optimal parameters extracted in the design of experiments. The raw materials used in the composite fabrication are carbon fiber and epoxy resin, with its properties specified in "Table 2". To form the mold, a

cylinder was made of aluminum according to the inner diameter of the chosen tube. To make it easy for the segment to get out of the mold, a 0.5-degree angle was applied to the wall of the cylinder.

First, the mold surface is thoroughly cleaned before fiber layup. Next, a release wax is used to easily separate the piece from the mold, stretched over the entire mold to a uniform thickness. Afterward, the resin-impregnated fabric was wrapped 26 times around the mold to obtain the desired thickness, i.e., 4 mm, by roll wrapping. After obtaining this thickness, the part is room temperature vulcanized. Ultimately, it was machined by the milling machine to obtain the desired length and damage initiation mechanism under an optimum angle (i.e., 45°). Figure 11 displays the constructed optimal specimen.

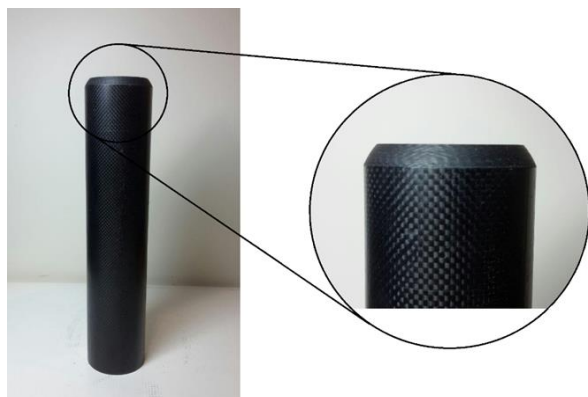


Fig. 11 Optimal specimen and damage mechanism under an optimum angle.

## 9 SPECIMEN EVALUATION

The specimen was subjected to quasi-static compression test after being prepared.

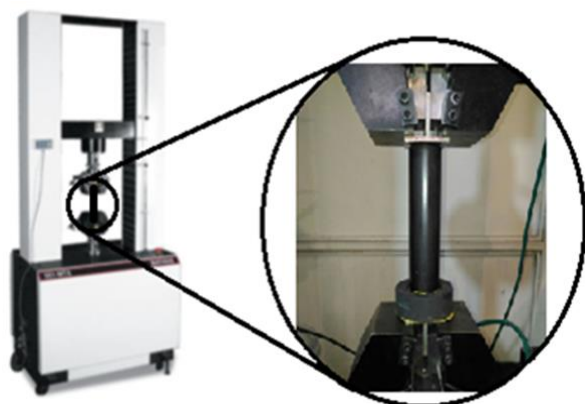


Fig. 12 Specimen mounting in the Santam S150 Tensile Testing Machine.

## 10 QUASI-STATIC COMPRESSION TEST

The Santam S150 Tensile Testing Machine was used to perform tensile testing. After the specimen was mounted between the two jaws, the upper jaw began to move, at a constant speed of 2 mm/min to apply the desired load. Figure 12 shows the specimen mounting in the Tensile Testing Machine.

## 11 RESULTS AND DISCUSSION

This section first attempts to make a comparison between the results of the simulated model and those of the study by Hong et al. Then, the results of the simulation of the quasi-static compression test of the specimens are expressed using the design of experiments. Finally, the results of the optimal specimen test are presented.

## 12 VALIDATION OF THE SIMULATED MODEL

Figure 13 shows the stress-displacement curve obtained from the experimental test performed by Hang as well as the simulated model. Moreover, Table 3 shows the output values obtained from the simulation and experimental tests. According to the results, the outputs of simulated model are close to those of the experimental work performed by Hong et al. The model can be used to optimize the energy absorber once it is validated.

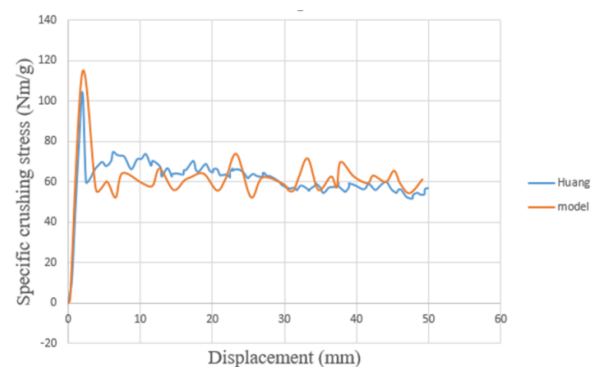


Fig. 13 Stress-displacement curve obtained from the experimental test performed by Hang and the simulated model.

Table 3 Output values from simulation and test

| SEA of the Simulated Model | SEA of the Experimental Study by Hong et al. | Percentage Error |
|----------------------------|--|------------------|
| 65.06 KJ/Kg                | 61.40 KJ/Kg                                  | 5.63%            |

### 13 SIMULATION RESULTS OF QUASI-STATIC COMPRESSION TEST PERFORMED ON COMPOSITE TUBE

After the tests, their outputs were fed into Design Expert software to extract the combined and independent effects of each of the input parameters (i.e., diameter-to-

height ratio, thickness-to-diameter ratio, and angle of damage initiation mechanism) on the output parameters (i.e., the specific energy absorption, average force, and maximum force). “Table 4” shows the method used to import data into the software. Figure 14 shows the optimal specimen under test.

**Table 4** Importing data into the Design Expert software

| un | Factor 1<br>A:D/L | Factor 2<br>B: t/D | Factor 3<br>C:Trigger an<br>degree | Response 1<br>SEA<br>Kj/Kg | Response 2<br>Pm<br>KN | Response 3<br>Pmax-Pm<br>KN |
|----|-------------------|--------------------|------------------------------------|----------------------------|------------------------|-----------------------------|
| 1  | 0.2               | 0.08               | 40                                 | 42.21                      | 25.21                  | 1.49                        |
| 2  | 0.15              | 0.08               | 40                                 | 40.41                      | 13.51                  | 1.56                        |
| 3  | 0.15              | 0.08               | 40                                 | 39.83                      | 13.68                  | 1.38                        |
| 4  | 0.1               | 0.06               | 20                                 | 29.36                      | 3.26                   | 2.19                        |
| 5  | 0.15              | 0.08               | 60                                 | 39.22                      | 13.16                  | 1.12                        |
| 6  | 0.15              | 0.08               | 40                                 | 39.91                      | 13.48                  | 1.54                        |
| 7  | 0.15              | 0.08               | 20                                 | 41.07                      | 14.63                  | 2.07                        |
| 8  | 0.1               | 0.08               | 40                                 | 38.52                      | 5.71                   | 1.43                        |
| 9  | 0.1               | 0.1                | 60                                 | 57.96                      | 10.15                  | 1.02                        |
| 10 | 0.15              | 0.08               | 40                                 | 40.21                      | 13.53                  | 1.45                        |
| 11 | 0.15              | 0.06               | 40                                 | 32.22                      | 8.23                   | 1.51                        |
| 12 | 0.2               | 0.1                | 20                                 | 62.42                      | 45.72                  | 1.98                        |
| 13 | 0.15              | 0.1                | 40                                 | 59.25                      | 24.33                  | 1.53                        |
| 14 | 0.15              | 0.08               | 40                                 | 40.07                      | 13.46                  | 1.46                        |
| 15 | 0.2               | 0.06               | 60                                 | 33.11                      | 15.26                  | 0.98                        |



**Fig. 14** Optimal specimen under test.

### 14 EFFECTS OF INPUT PARAMETERS ON THE RESULTS

After feeding the results of the simulated models into the Design Expert software, the effects of the input parameters on the output parameters derived from the Design Expert were extracted as a graph. Figure 15 shows the effects of the inner diameter-to cylinder height ratio on the SEA of the specimen. According to the graph, it is observed that the specific energy absorption increases with an increase in the inner diameter-to-

length ratio. Given a 12% change in the SEA for the L/D ratio between 0.1 and 0.2, this finding indicates a low dependence of the SEA on the L/D ratio. The SEA values obtained are relatively independent of the L/D ratio until the failure occurs continuously and gradually. This is in line with the research presented in Ref. [21].

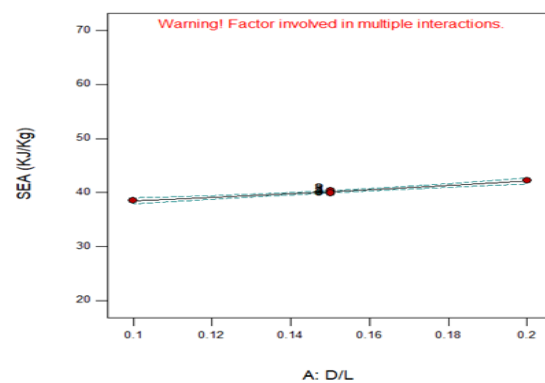


**Fig. 15** Effects of inner diameter-to-length ratio on the SEA.

Figure 16 shows the effects of the thickness-to-diameter ratio on the SEA. As can be seen, the SEA increases significantly with an increase in the thickness-to-diameter ratio, consistent with research by Hamannada [22].

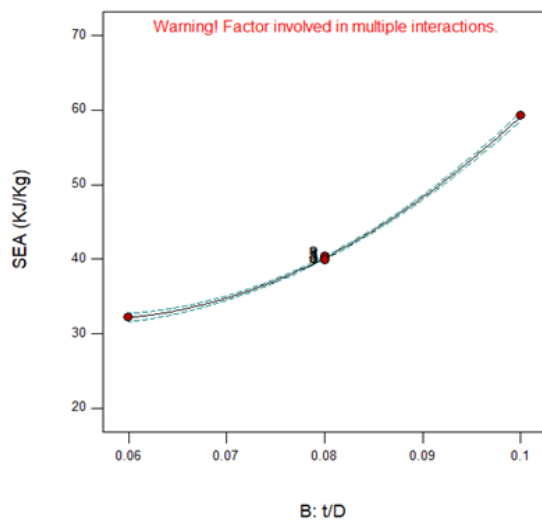


Fig. 16 Effects of thickness-to-diameter ratio on the SEA.

Figure 17 simultaneously shows the effects of the diameter-to-length ratio and thickness-to-diameter ratio relative to energy absorption. As indicated, the effects of the “thickness-to-diameter ratio” parameter are far greater than those of the “diameter thickness-to-length ratio” parameter.

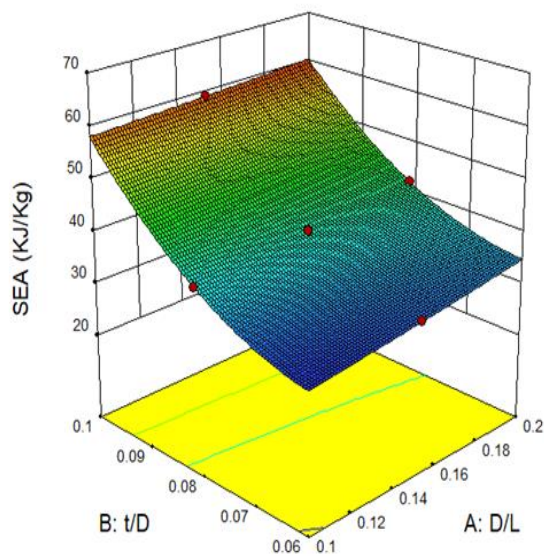


Fig. 17 Effects of diameter-to-length ratio and thickness-to-diameter relative to energy absorption.

Figure 18 shows the effects of the angle of the damage initiation mechanism on the SEA. As shown, the SEA remains almost constant with a slight decrease, with an increase in the angle from 20 to 60°.

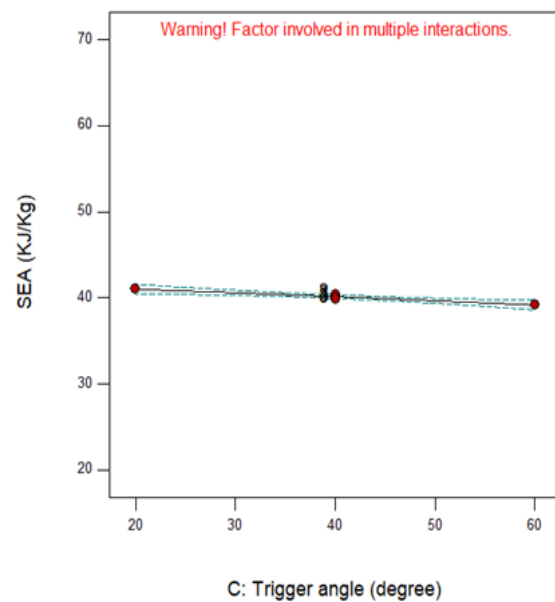


Fig. 18 Effects of the angle of damage initiation mechanism on the SEA.

Figure 19 shows the effects of the inner diameter-to-length ratio of the adsorbent on the average force. According to the graph, it is observed that the average force increases with an increase in the inner diameter-to-length ratio.

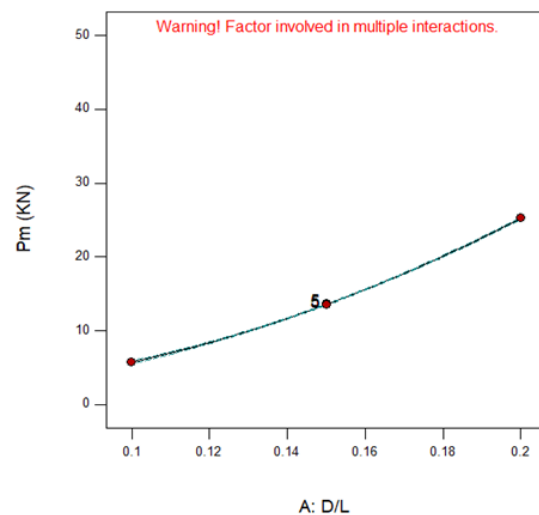


Fig. 19 Effects of inner diameter-to-absorber length ratio on the average force.

Figure 20 shows the effects of the thickness-to-inner diameter ratio on the average force. As illustrated, the average force significantly increases with an increase in the thickness-to-diameter ratio.

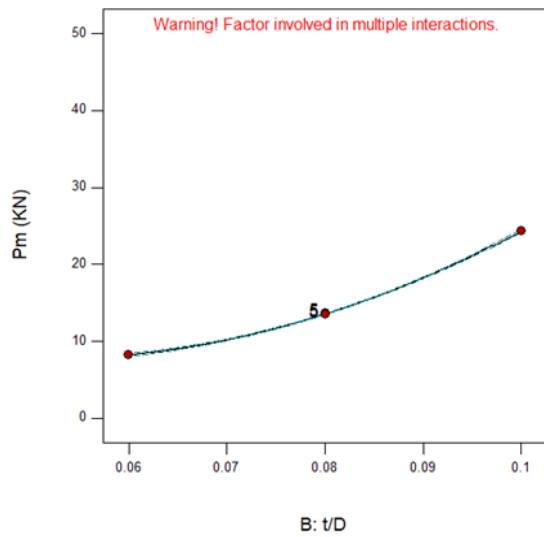


Fig. 20 Effects of thickness-to-inner diameter ratio on the average force.

Figure 21 shows the effects of the angle of the damage initiation mechanism on the average force. As we can see, the average force is almost constant with a slight decrease, with an increase in the angle from 20 to 60°.

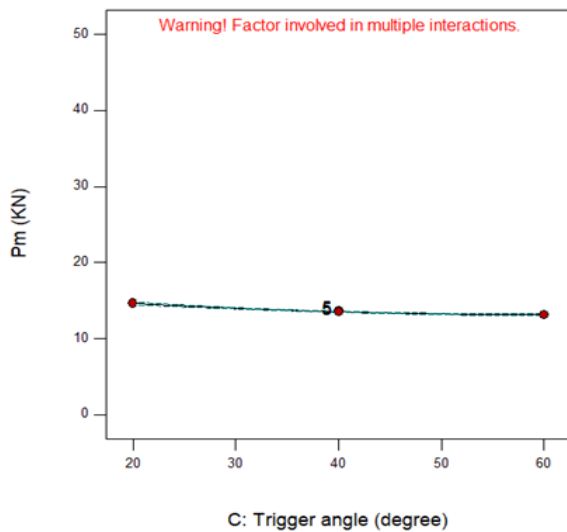


Fig. 21 Effects of the angle of damage initiation mechanism on the average force.

Figure 22 shows the effects of the angle of damage initiation mechanism on the difference between maximum force and average force. As demonstrated, the difference between maximum force and average force has been partially reduced, with an increase in the angle from 20 to 60°.

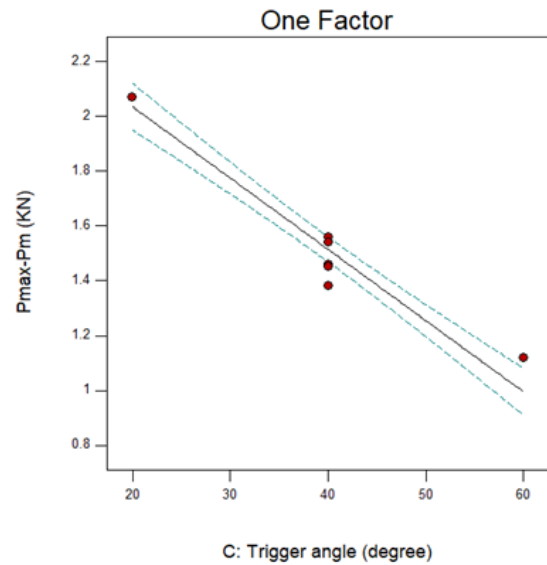


Fig. 22 Effects of the angle of damage initiation mechanism on the difference between maximum force and average force.

Then, the optimal specimen is selected after examining the effects of the parameters on the energy absorption properties. In terms of maximum SEA and average force and minimum difference between initial maximum force and average force, the optimal model proposed by Design Expert has the following properties: the inner diameter-to-length ratio of 0.2, thickness-to-inner diameter ratio of 0.1, and angle of damage initiation mechanism of 45°. Under these circumstances, taking into account the height of 200 mm for the cylinder height, the inner diameter is 40 mm and the thickness is 4 mm. In this case, the energy absorption is 61.36 kJ/kg, the average force is 42.98 kN, and the difference between the maximum force and the average force is 1.43 kJ. Figure 23 shows the force-displacement curve of this model.

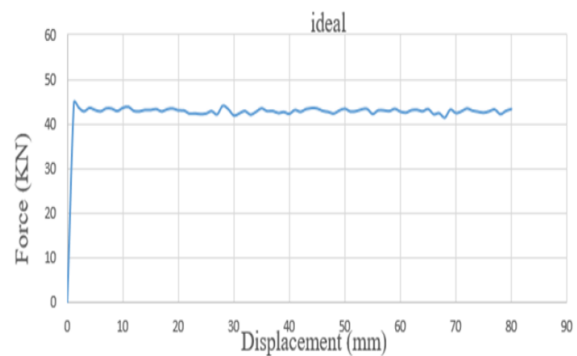


Fig. 23 Force-displacement curve of the designed optimal model.

In the end, according to the parameters selected for the optimal model, a specimen was made of carbon/epoxy with a length of 200 mm, an inner diameter of 40 mm, a thickness of 4 mm, and an angle of damage initiation mechanism of 45°. Thereafter, it was subjected to a quasi-static test with a constant displacement rate of 2 mm/min. According to the results, the energy absorption is 58.52 kJ/kg, the average force is 42.93 kN, and the difference between the maximum force and the average force is 1.72 kJ. Figure 24 shows the graph for this example.

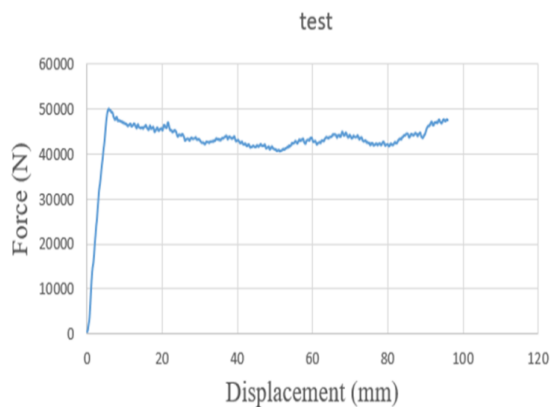


Fig. 24 Force-displacement curve of the ideal model.

Furthermore, “Table 5” shows the output values obtained from the simulation and experimental tests performed on the optimal model. The results suggest that the results obtained from the simulated model are close to those obtained from experimental work and they are valid.

Table 5 Output values obtained from simulation and optimal specimen test

| Output   | Simulated Optimal Model | Experimental Study of the Optimal Model | Percentage Error |
|--|-------------------------|---|------------------|
| SEA  | 61.36                   | 58.52                                   | 5.63%            |
| Average Force  | 42.98                   | 42.93                                   | 0.11%            |
| Difference between the maximum force and the average force | 1.43                    | 1.72                                    | 16.8%            |

## 15 CONCLUSION

This study aimed to design and fabricate a composite energy absorber applicable to passenger cars. Consequently, first, the quasi-static test and thin-walled

composite cylinder damage were simulated using Abaqus. Then, the results of this simulation were compared with those of an experimental study and validated. In the next step, several effective parameters in energy absorption were selected including outer diameter-to-cylinder height ratio, thickness-to-outer diameter ratio, and angle of damage initiation mechanism.

The adsorbent experiment was designed using RSM and modeled in Abaqus. These parameters were optimized and the optimum adsorbent sample was fabricated and tested. Optimal design parameters for improved energy absorption, increased average force, and reduced initial maximum force include inner diameter-to-cylinder height ratio of 0.2, thickness-to-inner diameter ratio of 0.1, and angle of damage initiation mechanism of 45°. Under these circumstances, the energy absorption is 58.52 kJ/kg, the average force is 42.93 kN, and the difference between the maximum force and the average force is 1.72 kN.

Given the above, this research is summarized as follows:

- In the case of separation failure, the smaller the radius of curvature of the openings and the greater the number of failures, the greater the energy absorption will be.
- With an increase in the angle from 20 to 60°, the SEA and average force remain almost constant along with a slight decrease.
- With an increase in angle from 20 to 60°, the difference between the maximum force and the average force is reduced.
- Optimal parameters for improved energy absorption, increased average force, and reduced initial maximum force, include inner diameter-to-cylinder height ratio of 0.2, thickness-to-inner diameter ratio of 0.1, and angle of damage initiation mechanism of 45°. Under these conditions, the adsorbent has an energy absorption of 58 kJ/kg, an average force of 42.93 kN, and the difference between the maximum force and the average force of 1.72 kN.

## REFERENCES

- [1] Farley, G.L., Wolterman, R. L., and Kennedy, J.M., Effects of Crushing Surface Roughness on the Crushing Characteristics of Composite Tubes, Journal of the American Helicopter Society, 1992, pp. 53-60.
- [2] Turner, Thomas, A., The Effects of Processing Variables On the Energy Absorption of Composite Crash Structures. PhD Thesis, University of Nottingham, 2004.
- [3] Hull, D., A Unified Approach to Progressive Crushing of Fiber Reinforced Composite Tubes. Composites Science and Technology, Vol. 35, 1993, pp. 231-246

- [4] Hamada, H., Ramakrishna, S., and Satoh, H., Crushing Mechanism of Carbon Fiber/ PEEK Composite Tubes. *Composites*, Vol. 26, 1995, pp. 749-755.
- [5] Nilson, S., Poly Ether Ether Ketone Matrix Resins and Composites. *International Encyclopedia of Composites*, Vol. 6, 1991, pp. 282.
- [6] Ramakrishna, S., Hamada, H., and Sato, H., Maekawa, Z., Energy Absorption Behavior of Carbon Fiber Reinforced Thermoplastic Composite Tubes, *Journal of Thermoplastic Composite Materials*, Vol. 1, 1995.
- [7] Sato, H., Hamada, H., Coppola, J. C., Hull, T. D., and Maekawa, T. Z., Comparison of energy absorption of carbon/epoxy and carbon/PEEK composite tubes, *Composites*, Vol. 23, No. 4, 1992, pp. 245-252.
- [8] Farley, G. L., Energy Absorption of Composite Material and Structures, Proc. 43rd American Helicopter Society Annual Forum, St. Louis, USA, 1987, pp. 613-627.
- [9] Farley G. L., Jones, R. M., Crushing Characteristics of Continuous Fiber- Reinforced Composite Tubes, *Journal of Composite Materials*, Vol. 26, 1992, pp. 37-50.
- [10] Hamada, H., Ramakrishna, S., Maekawa, Z., and Nakamura, M., Energy Absorption Behavior of Hybrid Composite Tubes, Proc. 10th Annual ASM/ESD Advanced Composite Conference, Dearborn, Michigan, USA, 7th–10th November 1994.
- [11] Ramakrishna, S., Hamada, H., Maekawa, Z., and Sato H., Energy Absorption Behavior of Carbon Fiber Reinforced Thermoplastic Composite Tubes, *J. Thermo. Comp. Mater.*, Vol. 8, 1995, pp. 323-344.
- [12] Gibson, R. F., Principles of Composite Material Mechanics, McGraw-Hill, Inc., 1994, pp. 364.
- [13] Brighton, M. Forrest, M. Starbuck, D. Erdman, and Fox, B., Strain Rate Effects on the Energy Absorption of Rapidly Manufactured Composite Tubes, *Journal of Composite Materials*, Vol. 43, No. 20, 2009, pp. 2183-2200.
- [14] Kindervater, C. M., Crash Impact Behavior and Energy Absorbing Capability of Composite Structural Elements, 30th International National SAMPE Symposium, 1985, pp. 19-21.
- [15] Pafitis D. G., Hull, D., Design of Fiber Composite Conical Components for Energy Absorbing Structures, *SAMPE Journal*, Vol. 27, 1991, pp. 29-34.
- [16] Fleming, D. C., Vizzini, A. J., Tapered Geometries for Improved Crashworthiness under Side Loads, *Journal of the American Helicopter Society*, January 1993, pp. 38-44.
- [17] Ochelski, S., Gotowicki, P., Experimental Assessment of Energy Absorption Capability of Carbon-Epoxy and Glass-Epoxy Composites, *Composite Structures*, Vol. 87, 2009, pp. 215-224.
- [18] D.C. Fleming, D. C., Vizzini, A. J., Tapered Geometries for Improved Crashworthiness Under Side Loads, *Journal of the American Helicopter Society*, January 1993, pp. 38-44.
- [19] Hannapel, F. W., Yuan, Y. B., Viegelahn, G. L., and Martin, C. D., Crashworthy Characteristics of Fiberglass / Polyester Frusta Under Quasi-Static Axial Loading, *Advanced Materials: New Developments and Applications Conference Proceedings*, 1991, pp. 469-479.
- [20] Jiancheng, H., Xinwei, W., Numerical and Experimental Investigations On the Axial Crushing Response of Composite Tubes Composite Structures, Vol. 91, 2009, pp. 222–22
- [21] Farley, G. L., Energy Absorption of Composite Material and Structure, 43rd American Helicopter Society Annual Forum, 1987, pp. 613-627.
- [22] Hamada, H., Ramakrishna, S., Scaling Effects in The Energy Absorption of Carbon-Fiber/PEEK Composite Tubes, *Composites Science and Technology*, Vol. 55, No. 3, 1995, pp. 211-221.